Nocturnal cooling in Local Climate Zone: Statistical approach using mobile measurements

François Leconte, Julien Bouyer, Rémy Claverie

Nocturnal cooling in Local Climate Zone: statistical approach using mobile measurements

Francois Leconte[a,b,*], Julien Bouyer[b,*], Rémy Claverie[b]

[a] *Université de Lorraine, Inra, LERMaB, F-88000, Épinal, France*
[b] *Cerema Est, Team research group, F-54510, Tomblaine, France*

Abstract

Up-to-date climate scenarios warn that the frequency and intensity of heat waves are likely to increase in Europe during the twenty first century. In these circumstances, urban climate is progressively taken into account in urban planning processes, for instance using terrain classifications. The developed methodology involves the Local Climate Zone scheme (LCZ), which has been applied to Nancy, France. Mobile measurements campaigns have been performed using an instrumented vehicle in order to record daily air temperature dynamics, with a focus on the daily cooling period. So as to quantify LCZ cooling before and after sunset over several days, a climatic indicator called Normalized Cooling Rate (NCR) has been used. This study presents statistical regressions that have been performed between normalized cooling rate values calculated from field measurements and urban indicators. Results indicate that normalized cooling rates and most of the studied urban features are correlated. Regression model using sky view factor and distance to the city center seems enough accurate to estimate nocturnal cooling at the district scale.

Key words: Urban Heat Island, Air temperature, Mobile measurements, Nocturnal cooling, Local Climate Zone, Urban indicators, Regression analysis

*Corresponding authors

Email addresses: `francois.leconte@univ-lorraine.fr` (Francois Leconte), `julien.bouyer@cerema.fr` (Julien Bouyer), `remy.claverie@cerema.fr` (Rémy Claverie)

1. Introduction

Urban heat island (UHI), that is described as the air temperature difference between city centers and their surrounding rural areas, has been recognized since the 1970s (Oke, 1973) and is now a well studied anthropic climatic phenomenon (Arnfield, 2003) (Gartland, 2008). It has been identified as a major concern for public policies (Rizwan et al., 2008), for now and for the next decades when heat waves will be more frequent. UHI needs to be more documented and understood by planners in order to improve its integration in projects and applications, especially at the district scale (Grimmond et al., 2010) (Baklanov et al., 2018).

The UHI magnitude is both influenced by geographical parameters and meteorological conditions - that can be qualified as uncontrollable variables - and by city morphology, materials, land use and anthropogenic sources - that can be qualified as controllable variables (Rizwan et al., 2008).

In order to perform accurate city climate diagnosis, modelling approaches are improving continuously (Mirzaei, 2015). Surface Energy Balance in meteorological meso-scale models is the more relevant technique to deal with physical processes both from district to city scale (Grimmond et al., 2010) (Grimmond et al., 2011). However, these models require at least a high level of expertise held by researchers or technical engineers with a strong background in climatology, or even, depending on the accuracy of model parametrisation, well-supplied urban databases.

To take into account climate processes in a first approach, many empirical and statistical modelling of UHI have been investigated. Oke proposed a method to link UHI maximum intensity with population and incident wind, and improved it by a function of aspect ratio to include the impact of city morphology (Oke, 1987). This approach has been pursued by several studies involving sky view factor (Unger, 2004) (Svensson, 2004), a combination of urban indicators (Balázs et al., 2009) or hybrid method between meteorological data and urban indicators (Bernard et al., 2017).

Other researches have descriminated urban features using terrain classification such as the Urban Climate Zone (Oke, 2006) and more recently the Local Climate Zone (LCZ) scheme (Stewart and Oke, 2012) to characterize inner urban climate. Measurements campaigns have highlighted that LCZ demonstrate homogeneous thermal behavior (Leconte et al., 2015) (Stewart et al., 2013).

Decision makers are looking for models involving urban indicators that

provide quantitative information about thermal behavior of districts. This work aims to develop correlations between LCZ indicators and UHI descriptors. This paper adresses specifically the methodology of statistical analysis and the limits associated to the consistency of LCZ indicators.

2. Materials and methods

2.1. Mobile measurements within Local Climate Zone

2.1.1. Climate classification in Nancy

The conurbation of Nancy is located North East of France and numbers $286,000$ inhabitants. It has an area of approximately 270 km^2 and its elevation ranges between 190 meters and 420 meters. Regarding its geographic features, Nancy is surrounded by two plateaus located West and North East of the conurbation, and crossed by two water bodies from South East to North. The Great Nancy Area is located in the center of the Lorraine region, which exhibits an temperate climate without dry season (Class Cfb according to the Köppen-Geiger classification (Peel et al., 2007)).

The Local Climate Zones (LCZ) classification has been applied for the area of interest. The determination of LCZ is organized following a three-steps method. The contours of the LCZ have been determined based on land use and building height information as well as global knowledge of the experimental field. Over the conurbation of Nancy, 82 urbanized LCZ have been identified.

2.1.2. LCZ selection for the field experiment

Thirteen LCZ of similar elevation have been selected, representing five different LCZ types. Within these areas, seven urban indicators have been calculated, namely sky view factor, aspect ratio, mean building height, terrain roughness class, building surface fraction, impervious surface fraction and pervious surface fraction. Contours have been corrected and a LCZ type has been assigned to each of these thirteen LCZ regarding urban indicators values (Table 1). Residential areas of Nancy presents urban features at the edge between two LCZ types, namely "Open Lowrise" and "Sparsely Built". It appears that urban indicators calculations did not allow to choose between these two LCZ types, therefore three residential areas have been classified as dual type "Open Lowrise / Sparsely Built".

LCZ code	SVF (-)	AR (-)	H (m)	R (-)	Built (%)	Imper (%)	Per (%)	LCZ type (-)
OUE	0.53	1.00	15.7	7	40	42	18	2 (Compact Midrise)
CEN	0.58	0.95	16.8	7	49	41	10	2 (Compact Midrise)
TRM	0.55	0.88	15.3	7	38	38	24	2 (Compact Midrise)
NAT	0.66	0.32	16.5	7	18	52	30	5 (Open Midrise)
THL	0.64	0.54	13.4	7	28	26	46	5 (Open Midrise)
SMA	0.66	0.51	11.0	7	28	42	30	5 (Open Midrise)
MBR	0.82	0.16	8.8	6	27	53	20	8 (Large Lowrise)
PVE	0.83	0.11	6.0	6	24	51	25	8 (Large Lowrise)
JAR	0.75	0.20	4.8	5	22	18	60	6 / 9 (Open Lowrise / Sparsely Built)
SEI	0.75	0.16	5.0	6	19	22	59	6 / 9 (Open Lowrise / Sparsely Built)
PUL	0.74	0.16	5.7	6	20	22	58	6 / 9 (Open Lowrise / Sparsely Built)
CE1	> 0.9	< 0.1	< 1	3	0	1	99	D (Low Plants)
CE3	> 0.9	< 0.1	< 1	3	0	1	99	D (Low Plants)

Table 1: Urban indicators values for the thirteen selected LCZ. SVF: Sky view factor, AR: Aspect ratio, H: Mean building height, R: Terrain roughness class, Built: Built surface fraction, Imper: Impervious surface fraction, Per: Pervious surface fraction.

2.1.3. Field survey with instrumented vehicle

On the basis of this LCZ map, screen-height air temperature has been recorded within these thirteen LCZ during summer 2013 and 2015 (Figure 1). Mobile measurements have been performed using an instrumented vehicle that records air temperature every three meters. A PT100 probe has been placed within a ventilated cylinder, which has been mounted on the roof of the car. This probe has an elevation of two meters above the ground, and an accuracy of 0.2 ℃. Data corresponding to very low speed measurements may be influenced by heat release from other vehicles, therefore measures carrier out below 15 $km.h^{-1}$ are dismissed. Since the itinerary is mostly urban, the maximum vehicle speed is around 60 $km.h^{-1}$. A sensitivity test has been performed in order to study the impact of vehicle speed on air temperature. Results demonstrate that mean air temperature values are marginally impacted by vehicle speed.

The chosen meteorological conditions are low wind speed (below 9 $m.s^{-1}$, wind speed at 10 m high), clear sky (from 0 to 2 octas), anticyclonic conditions, dry road and absence of precipitation during the previous twenty-four hours. Regarding these requirements, seven measurements days have been selected. Two measurements hours have been set, which correspond approximately to the beginning of the cooling phase (5 PM local time) and to the expected urban heat island amplitude maximum (three to five hours after sunset, 0 PM local time) (Oke, 1987). A measurement takes approximately two hours and thirty minutes, and during this time the regional temperature can decrease up to 2 ℃ at night. A linear time-correction scheme has been applied in order to balance the temperature evolution between the beginning and the end of the measure session. The scheme consists in correcting the measured air temperature proportionally to the elapsed time between the beginning of the session and the measurement.

2.2. Nocturnal cooling indicator at district scale

This study focuses on the air temperature behavior at the individual Local Climate Zones unit, which means that spatially averaged air temperature is considered. The spatial homogeneity inside LCZ has been analyzed in previous study (Leconte et al., 2015). The daily air temperature cycle is specially investigated. The air temperature difference between two Local Climate Zones is often used to characterize their thermal pattern. However, temperature difference only provides information at a given time of the day. In order to analyse the evolution throughout the time, heating rates or cooling

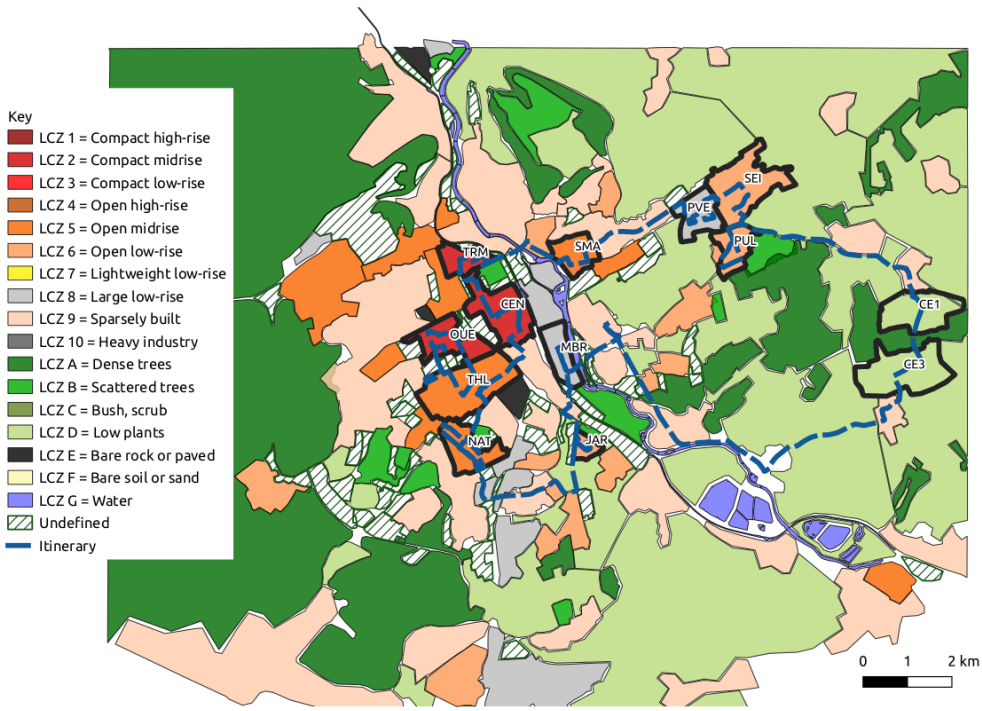

Figure 1: LCZ map of the Great Nancy Area. The itinerary is displayed in blue. The thirteen selected LCZ for the field experiment are circled in black.

rates can be implemented. These rates are calculated as the derivative of air temperature by the time.

Heating and cooling rates can be considered as urban climatic indicators to examine the urban heat island phenomenon. For city located in the same climate than Nancy, the urban heat island amplitude is generally weak during daytime and strong during nighttime. This phenomenon starts to develop before sunset and reach a maximum at night. Therefore, the cooling period is a relevant period to study the urban heat island. For low cloud cover and low wind speed, Holmer has observed that the cooling of neighborhoods is divided into two different phases (Holmer et al., 2007). During a first phase, urban areas show different cooling dynamics while during the second phase, the air temperature dynamics tend to be uniform between urban zones. The first phase coincides with a time period between one to two hours before sunset and three to five hours after sunset (P1 on Figure 2), while the second phase covers a period between three to five hours after sunset to sunrise (P2 on Figure 2). This two-phases cooling has been observed for several locations, namely in Singapore (Chow and Roth, 2006), Adelaide, Australia (Erell and Williamson, 2007), Athens, Greece (Giannopoulou et al., 2010), Ouagadougou, Burkina Faso (Holmer et al., 2013), Novi Sad, Serbia (Milosevic et al., 2019), and Nancy, France (Leconte et al., 2017). These previous results highlight that the amplitude of the urban heat island rises during phase 1 and remains stable during phase 2. Neighborhoods demonstrate different cooling rates during phase 1 and similar cooling rates during phase 2. In order to explicit the thermal behavior of Local Climate Zones during the development of the urban heat island, cooling rates during phase 1 are examined. The cooling rate are calculated between the daytime measure (character D on Figure 2) and the nighttime measures (character N on Figure 2). They are defined as :

$$\chi_{DN} = \frac{\Delta T_{air,DN}}{\Delta t_{DN}} \tag{1}$$

With Δt_{DN} the elapsed time between the two measures and $\Delta T_{air,DN}$ the air temperature decrease between the two measures for a given LCZ.

The diurnal temperature range (DTR) is expressed as the temperature difference between daily maximum and daily minimum temperature. It appears that cooling rates are not identical from one day to another due to diurnal temperature range variation. Thus, cooling rates during phase 1 have been normalized in order to be able to compare them when several days show dissimilar DTR values. When several Local Climate Zones are studied,

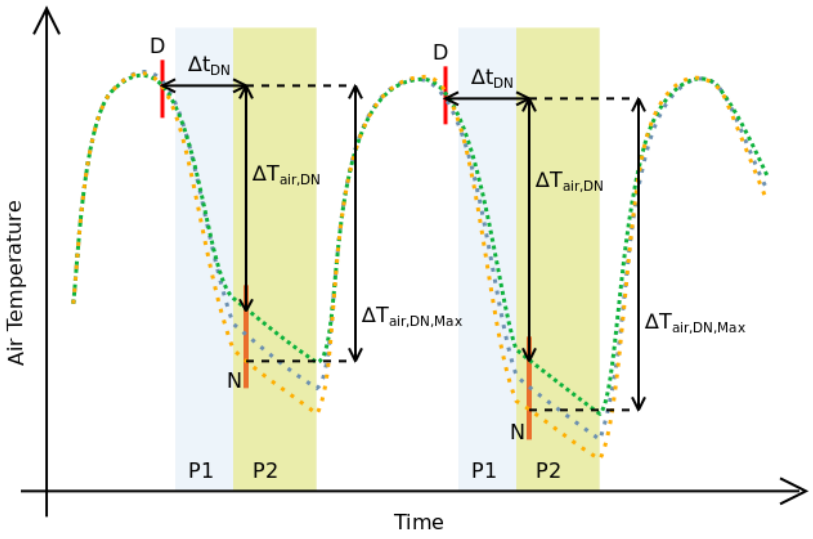

Figure 2: Theoretical nocturnal cooling phases for three LCZ of different types. Phase 1 (P1,blue area) is between 1 to 3 h before sunset and 3 to 5 h after sunset. Phase 2 (P2, green area) is between 3 and 5 h after sunset and sunrise. The letter D refers to the sessions performed in the middle of the afternoon, letter N refers to the sessions carried out around 3 h after sunset.

the cooling rates are divided by the temperature drop observed in the coolest Local Climate Zone during phase 1 ($\Delta T_{air,DN,max}$). In this way, all cooling rates – named normalized cooling rates (NCR) – are expressed relatively to an identified reference, namely the coolest studied area :

$$NCR = \frac{\chi_{DN}}{\Delta T_{air,DN,max}} \tag{2}$$

2.3. Statistical approach

In order to question the existence of a linear relationship between normalized cooling rate and urban indicators (UI), a regression analysis (ordinary least squares method) has been carried out. The regression model is evaluated by using both the regression coefficient to estimate the linearity and the Breusch-Pagan test to check if the variance around the regression line is the same for all values of the predictor (homoscedasticity) (Breusch and Pagan, 1979).

Nine urban indicators have been selected. Seven of them belong to the LCZ scheme, namely sky view factor (SVF), aspect ratio (AR), mean building height (H), terrain roughness class (R), building surface fraction (Built), impervious surface fraction (Imper), pervious surface fraction (Per). In addition, the distance to the center of the conurbation (Pos) and the elevation (Elev) have also been examined, as they may impact the thermal behavior of the districts. The statistical results have been evaluated according three criteria:

- The regression coefficient of the linear regression between NCR and one (or more) urban indicator is used to evaluate the regression quality. A correlation coefficient close to one corresponds to an accurate regression model.

- Akaike Information Criteria (AIC) is applied on regression equations in order to compare them. This criterion is defined as equation (3). (Akaike, 1981) (Akaike, 1998)

$$\mathrm{AIC} = 2K - 2\log(\ell(\widehat{\theta}|y)) \tag{3}$$

  Where K is the number of parameters to be estimated and $\log(\ell(\widehat{\theta}|y))$ is the log likelihood at its maximum likelihood estimator $\widehat{\theta}$ based on y observations. The most effective model is the model with the lowest

AIC score. This approach has been used in previous studies for statistical model selection, including in the geosciences field (Gopalan et al., 2018) (Bernard et al., 2017).

- Student's t-test has been performed for each UI's coefficient of the linear regression in order to evaluate their contribution. The significance threshold chosen for the P-value is 0.05.

Regression calculations have been completed over a sample representing 75% of the normalized cooling rate values which has been chosen randomly. The remaining values (25% of the experimental data set) have been used to examine the quality of the regression equation. Thus, NCR estimations from empirical models are compared with independent NCR observations. The goodness of fit is estimated with the Chi-Square statistic (eq 4). As depicted in this equation, the Chi-Square statistic (χ^2) is based on the difference between the NCR observed during field measurements and the NCR estimated using the statistical models.

$$\chi^2 = \sum \frac{(NCR_{Obs.} - NCR_{Est.})^2}{NCR_{Est.}} \tag{4}$$

The lower the Chi-Square value, the better the NCR estimated value.

3. Results and discussion

3.1. Single urban indicator approach

Regressions have been performed between NCR and each of the nine studied urban indicator UI_i ($i \in [\![1, 9]\!]$), according to equation (5).

$$\mathrm{NCR} = \beta_0 + UI_i \cdot \beta_1 \tag{5}$$

The constants β_0 and β_1 are the intercept and the slope of the linear regression respectively.

The relationship between NCR and urban indicators have been investigated based on 75% of the 90 experimental data set which has been chosen randomly. Initial dataset included measurements performed during seven days within thirteen LCZ (91 NCR values). One NCR value has been removed from the dataset due to experimental dysfunction. In order to assess the accuracy of this approach, the impact of the sample selection on regression results have been analysed. Multiple samples have been chosen

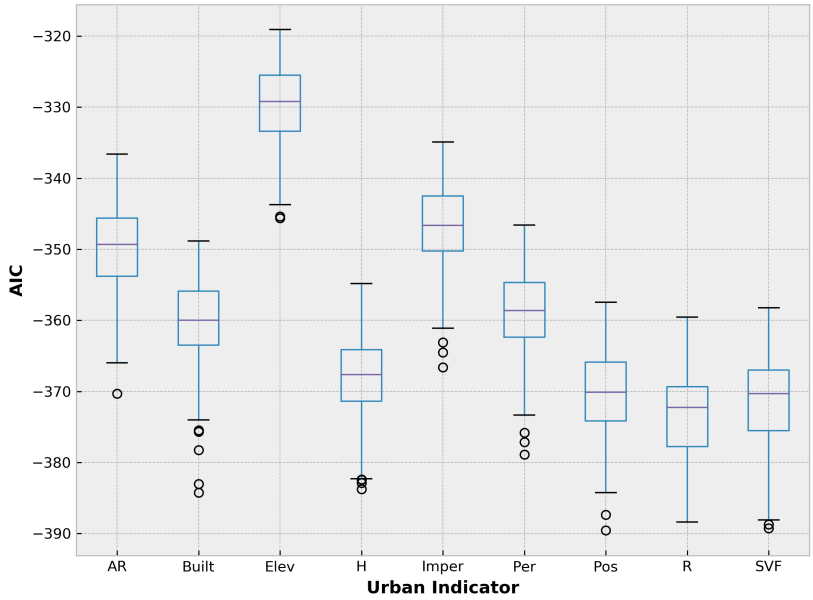

Figure 3: AIC values calculated from 180 different models for each urban indicator. Each model is based on 75% of the experimental data set which has been chosen randomly.

randomly and then used to perform regression between NCR and urban indicators. The number of random samples is twice larger than the amount of field observations.

Figure 3 highlights that terrain roughness class, sky view factor, mean building height and the distance to the center of the conurbation achieve the lowest AIC values. The box plots for each urban indicator tend to be similar in terms of interquartile range and distance between extremum values.

Overall, it seems that indicators related to the urban morphology perform better than land use indicators. Indeed, urban morphology indicators are ranked in 1^{st}, 2^{nd}, 4^{th} and 7^{th} positions in terms of AIC values, while land use indicators are ranked in 5^{th}, 6^{th} and 8^{th} positions.

After this step, one of the 180 random samples is selected, a regression is performed and it confirms the results of Figure 3 in terms of ranking. Table 2 summarizes the values of β_0 and β_1 coefficients as well as P-values, AIC and R^2 for one random sample. Thus, this sample will be used for following analysis. Results show that all Breusch-Pagan values are positives, which demonstrate the homoscedasticity of the data. All coefficients pass the Student's t-test, except in the case of the elevation. Based on AIC and

Urban Indicator	β_0	P $> \|t\|$	β_1	P $> \|t\|$	AIC	R^2	P_{BP}
R	0.17	$< 10^{-3}$	-0.01	$< 10^{-3}$	-362.43	0.48	0.21
SVF	0.03	$< 10^{-3}$	0.10	$< 10^{-3}$	-359.22	0.45	0.31
Pos	0.09	$< 10^{-3}$	0.01	$< 10^{-3}$	-358.13	0.45	0.12
H	0.13	$< 10^{-3}$	-0.00	$< 10^{-3}$	-356.79	0.43	0.42
Per	0.09	$< 10^{-3}$	0.00	$< 10^{-3}$	-350.83	0.38	0.20
Built	0.13	$< 10^{-3}$	-0.00	$< 10^{-3}$	-350.24	0.38	0.38
AR	0.12	$< 10^{-3}$	-0.04	$< 10^{-3}$	-341.93	0.29	0.85
Imper	0.13	$< 10^{-3}$	-0.00	$< 10^{-3}$	-340.39	0.28	0.28
Elev	0.02	0.59	0.00	0.01	-324.80	0.09	0.07

Table 2: Coefficients (β_0 and β_1), Student's t-test ($P > |t|$), Akaike Information Criteria and R^2 regarding regressions between normalized cooling rate and nine explanatory variables. Student's t-test results need to be under the chosen threshold of 0.05, whereas Breusch-Pagan values must be different from zero.

R^2 values, the terrain roughness class is the indicator that leads to the best correlation with normalized cooling rate values (AIC $= -362.4, R^2 = 0.48$), followed by the sky view factor (AIC $= -359.2, R^2 = 0.45$) and the distance to the center of the conurbation (AIC $= -358.1, R^2 = 0.45$). The model that achieves the best results is presented in equation (6).

$$\mathrm{NCR} = 0.17 \cdot \mathrm{R} - 0.001 \tag{6}$$

Scatter plots of experimental data including regression lines are presented (Figure 4). Each graph presents NCR values, in relation to urban indicators calculated within the each of the thirteen identified LCZ, for seven days of measurements. First, a significant dispersion of NCR values can be noticed for each of the urban indicators, between 0.04 and 0.06 h^{-1}. Nonetheless, all the scattered charts show trends of monotonic increase or decrease, except for the elevation indicator ($\mathrm{R}^2 = 0.09$) mostly because the measurement surveys have been carried out at almost constant elevation. This allows us to elaborate basic conclusions confirming previous studies which express local intensity of heat island as a linear function of the SVF (Svensson, 2004). The graphs show patterns of vertical alignments of dots corresponding to the seven days of measurements in each of thirteen LCZ. For several indicators such as AR, SVF or Imper, clusters can be perceived because same LCZ typologies lead to very close indicator values (cf. Table 1). This is even more obvious for R that shows only four distinct values of terrain roughness class. Indeed, R is calculated using the Davenport classification (Davenport et al., 2000),

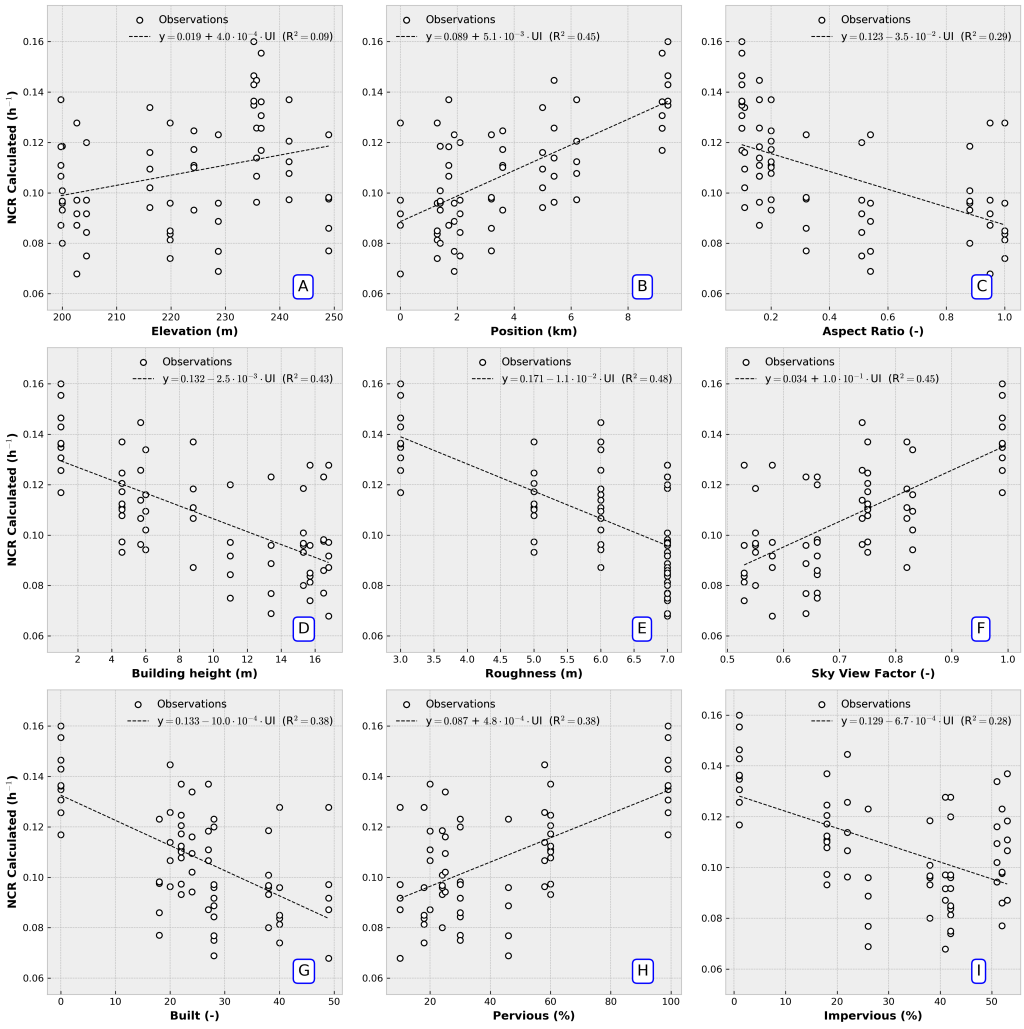

Figure 4: Scatter plots of experimental data including regression lines. Each observation correspond to a particular day for a given LCZ. Values with identical abscissa refer to a specific LCZ.

which implies that R values are integers (cf. Table 1). The thirteen studied LCZ in Nancy belong to only four roughness class. On the other hand, for the position indicator, a slightly more homogeneous horizontal distribution can be observed, except for the two LCZ D (Low plants) located at the outskirt of the city.

In order to evaluate the regression equation related to the urban indicators, NCR computed from statistical regressions has been confronted with NCR obtained from the measurement validation data set (Figure 5). χ^2 values are also calculated. The lower the χ^2 value, the closer the points from the first bisector. For the nine models, χ^2 values range from 0.02 to 0.065. The best results are obtained for the Sky View Factor (0.02), the distance to the center (0.02), the mean building height (0.022) and the terrain roughness class (0.022). Results presented in Figure 5 are consistent with AIC and R^2 values. Indeed, urban indicators with the lowest AIC values and the highest R^2 show the lowest χ^2 values. The elevation of all the studied LCZ is quite similar. Since the NCR varies depending on the LCZ, the regression between NCR and Elev leads to poor results. Thus, the parameter Elev will not be taken into account for the following section.

Finally, the single urban indicator approach allows to identify urban indicators that explain best the NCR variations. However, nocturnal cooling of LCZ is led by multiple factors. Therefore, a multiple urban indicators approach have to be investigated in order to propose a more comprehensive model.

3.2. Multiple urban indicators approach

Multiple linear regression are investigated between NCR and several urban indicators (Eq. (7)).

$$\mathrm{NCR} = \beta_0 + \sum_{p=1}^{p=n} UI_p \cdot \beta_p \tag{7}$$

A collinearity analysis of the urban indicators is carried out. A strong level of collinearity between independent variables can lower the performance of the statistical model. Correlation matrix between the eight urban indicators has been calculated (Figure 6). 82% of the correlation coefficients are above 0.7, which highlights that many indicators are strongly correlated.

The high level of correlation observed in Figure 6 is explained by the morphological and layout patterns of the neighborhoods. Indeed, an increase

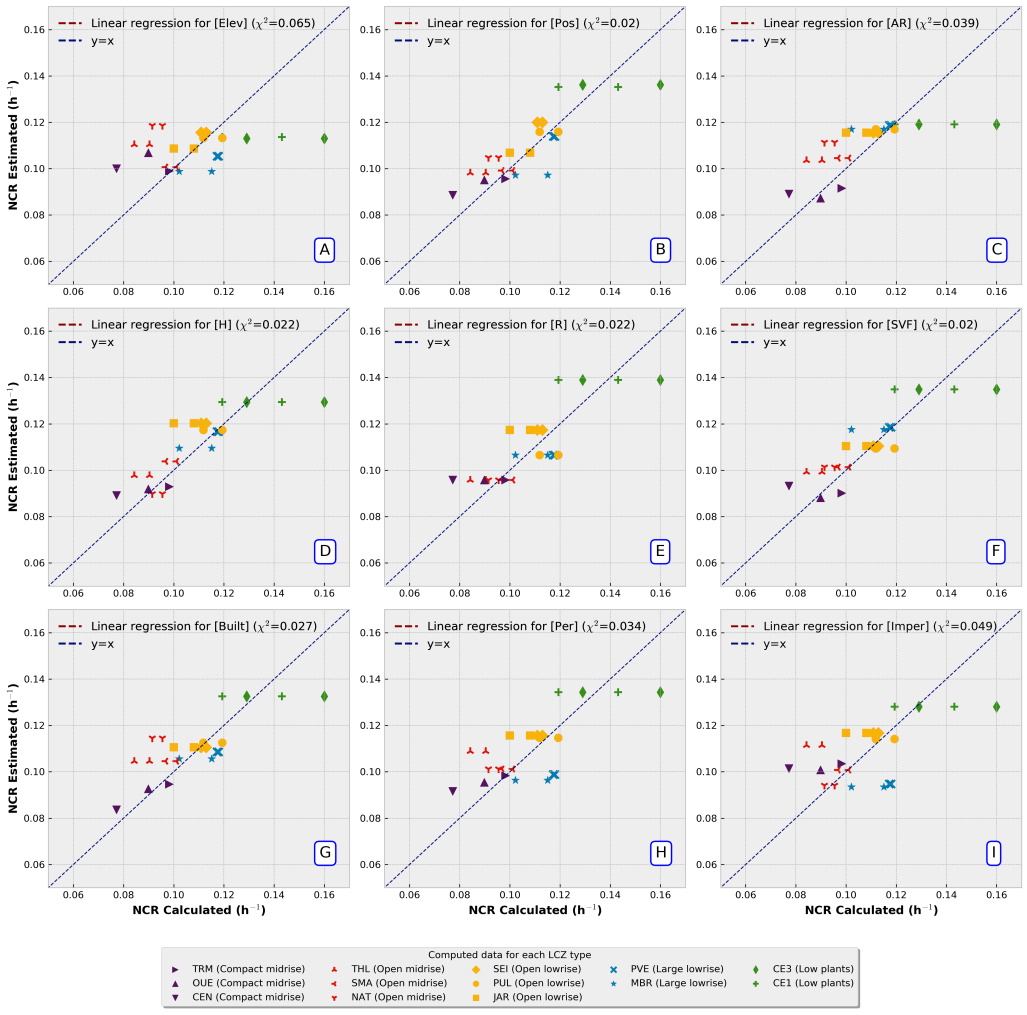

Figure 5: NCR from statistical regressions compared with NCR from the validation data set for single indicator regression. If the models would estimate perfectly the NCR from the validation data set, all the points would be on the first bisector (blue dashed line).

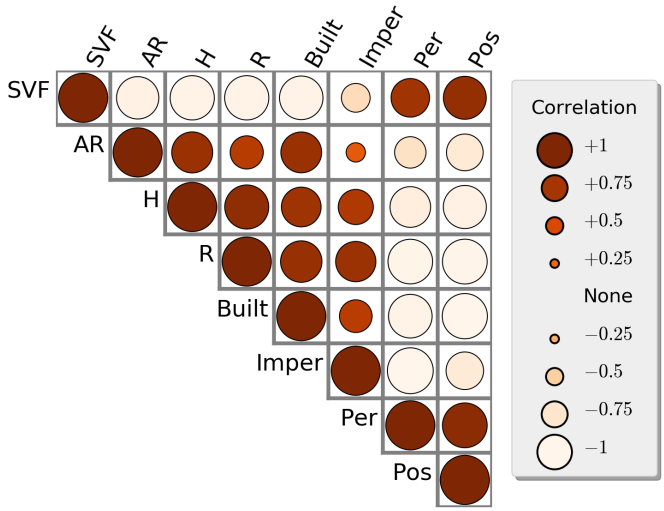

Figure 6: Correlation matrix of the explanatory variables, namely the urban indicators. The bigger the dot, the larger the correlation coefficient. The color indicates the sign of the correlation (positive/negative).

of sky view factor value may be linked to a decrease of built surface fraction and mean building height. The LCZ position in the conurbation (Pos) is also correlated with morphological and land use indicators. This result may be due to the specific spatial distribution of the LCZ types for the studied area. Within the Nancy conurbation, the most dense areas with highest building height and built surface fraction are located in the center, while the less dense areas with moderate building height and low built surface fraction can be found close to the conurbation's boundaries. Therefore, an increase of the radial distance from the center of the conurbation can correspond to an urbanisation gradient.

Explanatory variables can be considered as weakly correlated if the correlation coefficient ranges between -0.5 and $+0.5$. It appears that only one pair of urban indicators reaches this criteria, namely the impervious surface fraction with the aspect ratio. However, regarding the single indicator approach (cf. Section 3.1 and Table 2), these two indicators demonstrate poorer correlation with NCR (higher AIC and lower R^2) than other indicators. As a result, this pair (i.e. impervious surface fraction and aspect ratio) seems to be not relevant for a regression involving two indicators.

This analysis suggests that in the case of multi indicator regression, only a small number of urban indicators can be selected in order to lower the negative effects of the collinearity. The choice of these urban indicators is based on urban and statistical criteria.

First, it appears that urban indicators can be sorted depending on their nature. Sky view factor, aspect ratio, mean building height and terrain roughness class are related to the urban morphology, while the built, impervious and pervious surface fraction refer to the urban land use. The distance to the center of the conurbation can be considered as independent geographical indicator. If the two urban indicators selected for the regression belong to the same group, the model may be redundant and the other group will not be represented. Therefore, the two selected indicator should be chosen in different groups.

Second, indicators that demonstrate low AIC values for single indicator regression can be selected for multiple variables regression. For the land use group, the pervious surface fraction has been selected. Unlike the built and impervious surface fraction, this indicator provides an indirect information regarding the vegetation. Regarding the urban morphology group, R and SVF show the best AIC values. The later is selected for the multiple indicator regressions because it describes the urban geometry in a more detailled way than the terrain roughness class, which is based on the Davenport classification. The distance to the center has been selected due to its low AIC value.

Three urban indicators – namely SVF, Per and Pos – are then selected to carry out regressions. Four regressions are presented, namely:

- Three regressions between NCR and two explanatory variables (combinations of SVF, Per and Pos)
- One regression between NCR and three explanatory variables

Models are discussed regarding their χ^2 value (cf. section 2.3). Figure 7 presents NCR calculated from the observations in function of NCR estimated by regressions in the multiple variables regression case. χ^2 ranges from 0.016 to 0.02. Among the two indicators model, the pair SVF and Pos obtains the lowest χ^2 value (0.016). This can be considered as an improvement regarding the single variable regression approach, which only reach a χ^2 value of 0.02. Finally, the two indicators model which leads to the better estimation of the

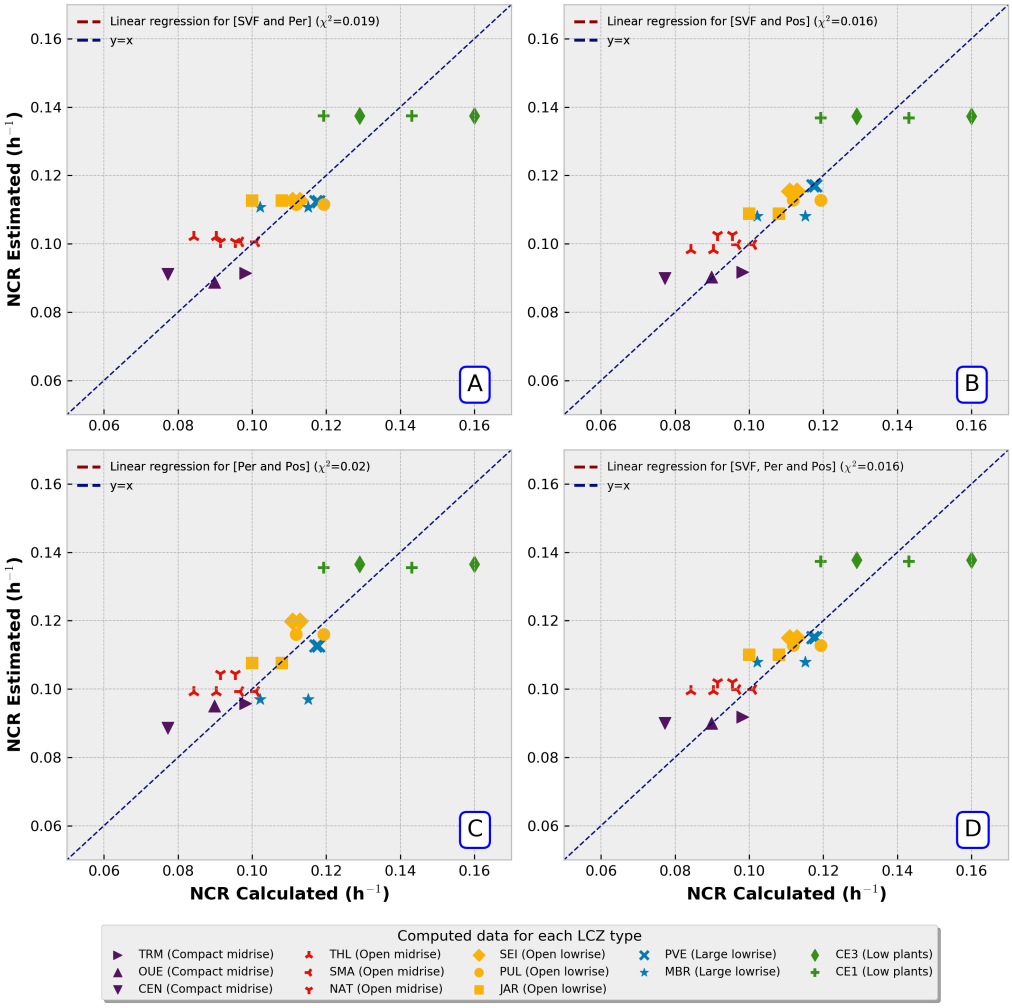

Figure 7: NCR from statistical regressions compared with NCR from the validation data set for multiple indicator regression. If the models would estimate perfectly the NCR from the validation data set, all the points would be on the first bisector (blue dashed line).

normalized cooling rate is expressed in equation (8).

$$NCR = 4.7 \times 10^{-3} \cdot Pos + 4.4 \times 10^{-5} \cdot Per + 8.8 \times 10^{-2} \quad (8)$$

In addition, a model involving these three indicators is proposed. Regression model involving three urban indicators – namely SVF, Per and Pos – do not achieve better performance ($\chi^2 = 0.016$).

4. Conclusion

This paper questions the relationship between the cooling pattern of districts and several urban indicators. This study has required the application of the Local Climate Zone scheme in Nancy. During this stage, nine urban indicators have been determined within a selection of thirteen LCZ. Nocturnal cooling information has been gathered throughout measurement campaigns, and normalized cooling rate have been calculated based on these field data.

The statistical connection between NCR and the chosen urban indicators has been investigated using regression analysis. The statistical models are built using 75% of the total experiments. The overall performance of the urban indicators (i.e. AIC values) is independent from the sample. Nine single variable regressions are presented. Terrain roughness class, the sky view factor, the mean building height and the distance to the center of the conurbation achieve best results in terms of AIC, R^2 and χ^2.

Multi indicator regressions have been investigated in order to take into account multiple drivers of the LCZ nocturnal cooling. Correlations appear to be generally strong between urban indicators, which limits the number of explanatory variables for the regression. Three urban indicators are selected for the multiple indicator regression. The best results are obtained with the pair SVF and Pos. The addition of a third explanatory variable do not improve the performance of the model.

Regression analysis underlines the general trends regarding the relationship between normalized cooling rate and the nine selected urban indicators. Overall, it looks like NCR and most of the studied urban features are correlated. However, morphological indicators seems to perform better than land use indicators.

Acknowledgments

This work has been supported by the French Environment and Energy Management Agency (ADEME).

References

Akaike, H., 1981. Likelihood of a model and information criteria. Journal of Econometrics 16 (1), 3 – 14.

Akaike, H., 1998. Information Theory and an Extension of the Maximum Likelihood Principle. Springer New York, New York, NY, pp. 199–213.

Arnfield, A., 2003. Two decades of urban climate research: a review of turbulence, exchanges of energy and water, and the urban heat island. International Journal of Climatology 23, 1–26.

Baklanov, A., Grimmond, C., Carlson, D., Terblanche, D., Tang, X., Bouchet, V., Lee, B., Langendijk, G., Kolli, R., Hovsepyan, A., 2018. From urban meteorology, climate and environment research to integrated city services. Urban Climate 23, 330 – 341, iCUC9: The 9th International Conference on Urban Climate.

Balázs, B., Unger, J., Gál, T., Sümeghy, Z., Geiger, J., Szegedi, S., 2009. Simulation of the mean urban heat island using 2D surface parameters: empirical modelling, verification and extension. Meteorological Applications 16, 275–287.

Bernard, J., Musy, M., Calmet, I., Bocher, E., Keravec, P., 2017. Urban heat island temporal and spatial variations: Empirical modeling from geographical and meteorological data. Building and Environment 125, 423 – 438.

Breusch, T. S., Pagan, A. R., 1979. A simple test for heteroscedasticity and random coefficient variation. Econometrica 47 (5), 1287–1294.

Chow, W., Roth, M., 2006. Temporal dynamics of the urban heat island of Singapore. International Journal of Climatology 26, 2243–2260.

Davenport, A., Grimmond, C., Oke, T., Wieringa, J., 2000. Estimating the roughness of cities and sheltered country. In: Proceedings of the 12th Conference of Applied Climatology.

Erell, E., Williamson, T., 2007. Intra-urban differences in canopy layer air temperature at a mid-latitude city. International Journal of Climatology 27, 1243–1255.

Gartland, L., 2008. Heat Island : Understanding and Mitigating Heat in Urban Areas. Earthscan.

Giannopoulou, K., Santamouris, M., Livada, I., Georgakis, C., Caouris, Y., 2010. The impact of canyon geometry on intra urban and urban suburban night temperature differences under warm weather conditions. Pure and Applied Geophysics 167, 1433–1449.

Gopalan, S., Kawamura, A., Takasaki, T., Amaguchi, H., Azhikodan, G., 2018. An effective storage function model for an urban watershed in terms of hydrograph reproducibility and akaike information criterion. Journal of Hydrology 563, 657–668.

Grimmond, C., Blackett, M., Best, M., Baik, J.-J., Belcher, S., Beringer, J., Bohnenstengel, S., Calmet, I., Chen, F., Coutts, A., Dandou, A., Fortuniak, K., Gouvea, M., Hamdi, R., Hendry, M., Kanda, M., Kawai, T., Kawamoto, Y., Kondo, H., Krayenhoff, E., Lee, S.-H., Loridan, T., Martilli, A., Masson, V., Miao, S., Oleson, K., Ooka, R., Pigeon, G., Porson, A., Ryu, Y.-H., Salamanca, F., Steeneveld, G.-J., Tombrou, M., Voogt, J., Young, D., Zhang, N., 2011. Initial results from phase 2 of the international energy balance model comparison. International Journal of Climatology 31, 244–272.

Grimmond, C., Roth, M., Oke, T., Au, Y., Best, M., Betts, R., Carmichael, G., Cleugh, H., Dabberdt, W., Emmanuel, R., Freitas, E., Fortuniak, K., Hanna, S., Klein, P., Kalkstein, L., Liu, C., Nickson, A., Pearlmutter, D., Sailor, D., Voogt, J., 2010. Climate and more sustainable cities: climate information for improved planning and management of cities (producers/capabilities perspective). Procedia Environmental Sciences 1, 247–274.

Holmer, B., Thorsson, S., Eliasson, I., 2007. Colling rates, sky view factors and the development of intra-urban air temperature differences. Geografiska Annaler Series A - Physical Geography 89, 237–248.

Holmer, B., Thorsson, S., Lindén, J., 2013. Evening evapotranspirative cooling in relation to vegetation and urban geometry in the city of Ouagadougou, Burkina Faso. International Journal of Climatology 33, 3089–3105.

Leconte, F., Bouyer, J., Claverie, R., Pétrissans, M., 2015. Using Local Climate Zone scheme for UHI assessment: evaluation of the method using mobile measurements. Building and Environment 83, 39–49.

Leconte, F., Bouyer, J., Claverie, R., Pétrissans, M., Oct 2017. Analysis of nocturnal air temperature in districts using mobile measurements and a cooling indicator. Theoretical and Applied Climatology 130 (1), 365–376.

Milosevic, D., Savic, S., Arsenovic, D., Secerov, I., Matzarakis, A., 2019. Quantification of temporal changes of urban heat island intensity and cooling and heating rates in different local climate zones of mid-sized central european city (tromp foundation travel award). In: Proceedings of the EMS Annual Meeting 2019.

Mirzaei, P. A., 2015. Recent challenges in modeling of urban heat island. Sustainable Cities and Society 19, 200 – 206.

Oke, T., 1973. City size and the urban heat island. Atmospheric Environment (1967) 7 (8), 769 – 779.

Oke, T., 1987. Boundary Layer Climate, 2nd Edition. Routledge.

Oke, T., 2006. Toward better scientific communication in urban climate. Theoretical and Applied Climatology 84, 179–190.

Peel, M., Finlayson, B., McMahon, T., 2007. Updated world map of the Köppen-Geiger climate classification. Hydrology and Earth System Sciences 11, 1633–1644.

Rizwan, A., Dennis, Y., Liu, C., 2008. A review on the generation, determination and mitigation of urban heat island. Journal of Environmental Sciences 20, 120–128.

Stewart, I., Oke, T., 2012. Local Climate Zones for urban temperature studies. Bulletin of American Meteorology Society 93, 1879–1900.

Stewart, I., Oke, T., Krayenhoff, E., 2013. Evaluation of the 'Local Climate Zone' scheme using temperature observations and model simulations. International Journal of Climatology (DOI: 10.1002/joc.3746).

Svensson, M., 2004. Sky view factor analysis - implications for urban air temperature differences. Meteorological Applications 11, 201–211.

Unger, J., 2004. Intra-urban relationship between surface geometry and urban heat island: review and new approach. Climate Research 27, 253–264.